Fluidization Characteristics of Biobone Particles Used for Biocatalysts

N. Ellis, A. Margaritis, C. L. Briens, and M. A. Bergougnou
Dept. of Chemical and Biochemical Engineering, The University of Western Ontario, London, Ontario, N6A 5B9, Canada

Liquid–solid fluidization characteristics of irregularly shaped Biobone particles were studied in a fluidized bioreactor column 2.35 m high and 0.1 m dia. The wet biobone particles had a density of 1,890 kg/m^3. Two size ranges were studied: 1.70–2.36 mm and 1.25–2.36 mm. The Biobone is a natural cheap material composed of collagen, which is a strong protein structure, embedded with microcrystals of hydroxyapatite and calcium phosphate, and it is an excellent matrix of commercial importance used for the immobilization of enzymes, whole cells and other biocatalysts. Fluidization characteristics of Biobone particles, which include measurements of pressure drops, holdups, minimum fluidization velocities, particle entrainment, and residence time distributions at different water superficial velocities, are reported. Because of the highly irregular shape of Biobone particles, new fluidization behavior was observed, which was much different from the fluidization behavior of spherical particles reported in the literature. A new channeling index, I_c, is proposed to quantify the channeling characteristics of fluidized Biobone particles, and a new parameter, α, was developed to distinguish the transition between fixed and fluidized states of the Biobone particles.

Introduction

Fluidized bioreactor systems are rapidly emerging as important new components of many bioprocesses that employ immobilized enzymes, whole cells, or other subcellular organelles, as biocatalysts for the biotransformation of different materials. The advantages of fluidized bioreactors compared to traditional fixed-bed bioreactors include superior heat- and mass-transfer characteristics resulting from better mixing in two- and three-phase fluidized systems. In fixed-bed bioreactors using immobilized biocatalysts, one of the potential problems is the "fouling" or plugging of the void space between the fixed particles, which may create serious pressure drop and flow problems. A large number of solid particles and hydrogels have been used to immobilize the following biocatalysts: enzymes, whole cells, yeasts and other fungi, bacteria, plant cells, mammalian cells, or other subcellular fragments. The attachment or immobilization of these biocatalysts to the solid particles is achieved by different methods, which include, adsorption, covalent bonding, cross-linking, and physical entrapment in hydrogels (Margaritis and Merchant, 1984). Fluidized bioreactor systems are used in bioprocessing for the production of high-value medicinal products, ethanol and beer production, food processing and beverage, wastewater treatment, and other environmental applications (Margaritis and Wallace, 1984; Margaritis et al., 1987; Gee and Ramirez, 1994; Weuster-Botz, 1993; Fan, 1989; Merchant et al., 1987).

The physical and chemical properties of a solid matrix used to immobilize a biocatalyst are very important along with the fluidization characteristics of these solid particles in two- or three-phase applications. In this article we report the fluidization characteristics of irregularly shaped biobone particles, with water as the fluidizing liquid in a cylindrical column. Very few published results deal with the fluidization properties of nonspherical and irregularly shaped particles.

Biobone is a granular solid porous material derived from the bone byproduct resulting from the mechanical deboning of poultry, and it is a new immobilization matrix of industrial importance that has many superior characteristics compared to other existing immobilization materials (Ellis, 1993). The biobone product may be sized according to specification, and it is a very strong matrix with pore sizes ranging from 100 μm

Correspondence concerning this article should be addressed to A. Margaritis. Present address of N. Ellis: 3-4-9 Asahi-cho, Fuchu-shi, Tokyo 183, Japan.

μm, and can withstand high fluid pressures without compacting, with excellent flow characteristics.

Biobone is a natural matrix of very low cost and in abundant supply, and its chemical composition and physical strength make it an excellent immobilization matrix. Biobone is a composite matrix that is made of collagen, a strong protein structure, embedded with microcrystals of hydroxyapatite and calcium phosphate. The collagen protein network gives elasticity and cohesion to the biobone structure, and provides many binding sites, such as amino and carboxyl groups for covalent attachments of enzymes, and other biocatalysts. At the same time, the mineral content of biobone gives strength to the porous structure and the phosphates present carry a large number of charges that can be used for immobilization of enzymes, whole cells, and other biocatalysts by direct adsorption. Biobone is an inert natural material, nontoxic, inexpensive, of abundant supply, and can be used in many different pharmaceutical and food applications where immobilized biocatalysts are employed. Biobone has been used to immobilize different enzymes, and whole cells in food and other applications (Findlay et al., 1986; Manji et al., 1988; Negishi et al., 1989; Schafhauser and Storey, 1992).

Despite the commercial importance of biobone as an immobilization matrix and its use in fluidized bioreactors, no data exist in the literature on the solid–liquid fluidization characteristics of biobone with water as the fluidizing agent. In this article we report original results on the two-phase fluidization characteristics of biobone particles, which includes measurements of pressure drops, holdups, minimum fluidization velocities, particle entrainment, and channeling characteristics of the fluidized bioreactor system.

Equipment and Experimental Methods

Characterization of biobone particles

The biobone particles used in this study were crushed chicken bones supplied by Bioprotein Canada Inc., Hamilton, Ontario. The apparent density of wet biobone particles was measured by displacement and was found to be 1,890 kg/m^3 for all sizes. As shown in Figure 1, the biobone particles were flaky, highly nonspherical and needlelike. Their size and shape distributions were measured with a Brinkman Particle Size Analyzer (model PSA2010).

The raw biobone contained particles ranging in size from 0.1 to 5 mm. This made it very hard to achieve smooth fluidization without excessive particle entrainment. Sieving with regular, square-holed, metallic screens was therefore used to prepare two size fractions for fluidization: the first fraction contained particles ranging in "screen size" from 1.25 to 2.35 mm, while the second fraction contained particles ranging in "screen size" from 1.70 to 2.35 mm.

The terminal free-falling velocity of single particles was measured in a 45-cm-high column filled with a mixture of glycerin and water of a 0.003 Pa·s viscosity. Measurements were made once the particles had been fully accelerated and reached their terminal velocity. Although using the glycerin–water mixture greatly reduced the random error on the terminal velocity, it introduced a systematic error of about -10% when extrapolated to pure water conditions, according to the Haider–Levenspiel (1989) correlation.

The cohesivity of a powder can be evaluated from its angle of internal friction. The angle of internal friction of both dry and wet Biobone was measured by adding Biobone particles to a vertical cylindrical tube with a movable piston as its bottom. When a critical height of solids was reached, it became impossible to push up the piston. The internal friction angle was obtained from the arctangent of the ratio of the critical height to the tube diameter.

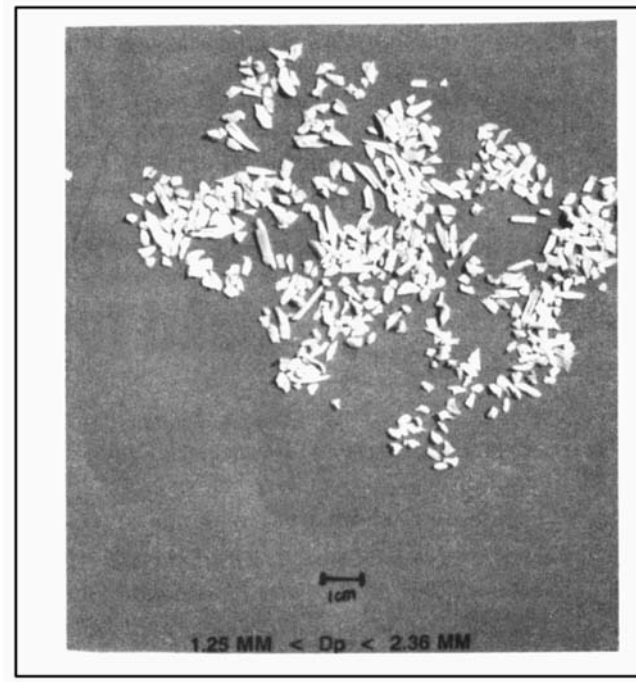

Figure 1. Biobone particles of sieve size distribution 1.25 mm to 2.36 mm.

Fluidized-bed column

The Altuglass fluidized-bed column, 2.35 m high and 0.1 m in dia., is shown in Figure 2. The liquid was distributed into the bed through a 3-mm-thick perforated grid with 160 holes of 1.5 mm dia. on a 7-mm pitch. This ensured good liquid distribution since the grid pressure drop was always at least 10% of the fluidized-bed pressure drop. The column was first tested with a bed of 2.5-mm glass beads and the distributor performed well: no channeling was observed. A cylindrical screen at the top of the column prevented any entrained particles from escaping the column.

The column was equipped with 15 pressure taps connected to water manometers as shown in Figure 2. Capillaries in the manometer tubes damped the manometer level fluctuations without affecting their average level. The pressure gradients and liquid holdups reported in this article were, thus, time-averaged.

The fluidizing liquid was tap water to which trace amounts of sodium hypochlorite were added to prevent bacterial growth on the Biobone particles. The liquid was circulated through a holding tank with a centrifugal pump and the flow rate was measured with on-line calibrated elbowmeters.

Particle entrainment measurements

To estimate the flux of particles entrained from the fluidized bed, a 65-mm-ID cup was located in the freeboard,

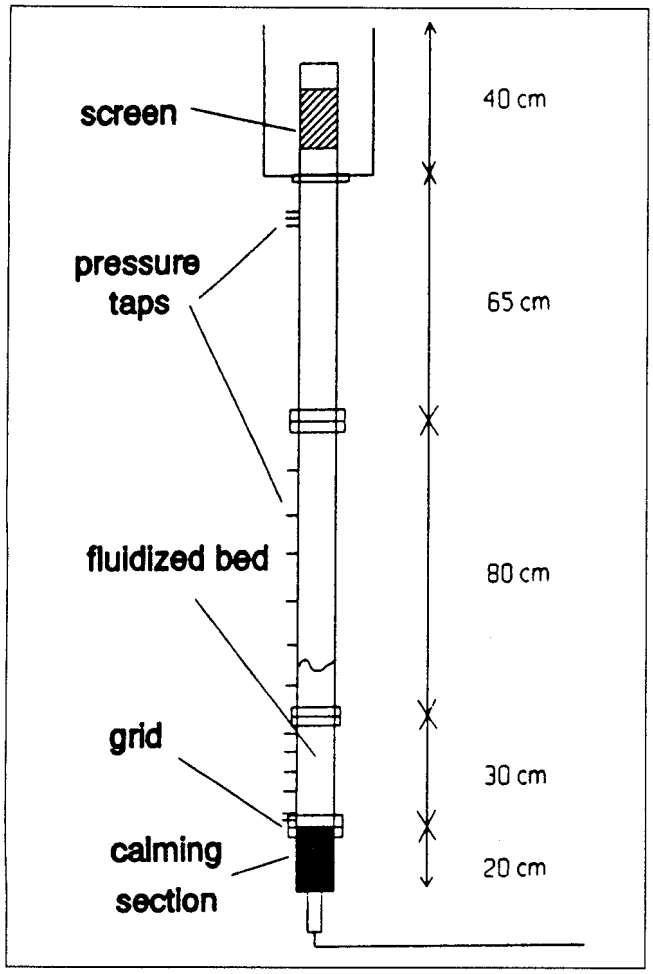

Figure 2. Fluidized bioreactor column.

1.34 m from the grid, with its mouth facing upward. Since the top of the column was fitted with a screen that prevented the entrained particles from escaping the column, the flux of particles collected by the cup corresponded to the flux of particles that would be lost from the column in the absence of a screen.

Liquid residence time distribution measurements

The liquid residence time distribution for the fluidized bed was measured by performing a downstep of sodium chloride tracer just above the grid and detecting the resulting tracer concentration change below the bed surface. To avoid concentration fluctuations, the tracer solution was saturated with sodium chloride. All fluidization experiments were performed at room temperature.

The tracer solution was injected with a sparger that spanned the column diameter and was located 3.5 cm above the grid. The sparger had an inner diameter of 3 mm and was equipped with five 0.16-mm-dia. holes. The pressure drop through the holes was such as to ensure equal tracer flow through each hole along the sparger tube. To achieve a perfect downstep, steady tracer flow through the sparger was established with a peristaltic pump. After an appropriate time of about 10 min, a three-way valve was rotated to simultaneously stop the tracer flow from the pump and reverse the flow through the sparger by connecting it to a vacuum flask (see Figure 3). The tracer injection system is shown in Figure 3.

The instantaneous tracer concentration was measured by electroconductivity at a level 36.5 cm above the grid. Two 1-cm-high-by-6-cm-wide electrodes made of platinized titanium mesh were fitted to the column wall at two diametrically opposite locations. This arrangement did not disturb the column hydrodynamics and measured the average tracer concentration over the entire column cross section. Galy-Jammou et al. (1995) demonstrated the reliability of such electrodes. To avoid polarization, an AC potential of 3.5 V was applied to the electrode. The intensity of the resulting current through the column was obtained from the potential drop across a calibrated 100-Ω resistance, which was sampled at a frequency of 500 Hz by a data acquisition system (see Figure 3). The signal amplitude was obtained by fitting a sinusoid to the digitized data according to the method reported by Del Pozo et al. (1992). The applied AC potential had a 60-Hz frequency, which meant that the measured impedance included a minor contribution from the column capacitance. Calibration runs with various sodium chloride concentrations established a linear relationship between salt concentration and the measured signal. The sodium chloride concentration was kept so low that it did not appreciably affect the bed hydrodynamics (Del Pozo et al., 1994).

Six replicate downstep experiments were performed for each set of hydrodynamic conditions and the average of the resulting signals yielded the residence time distribution. The replicate experiments were needed because the liquid circulation patterns oscillated slightly with time. Although fluctuations in the local cross-sectional average of the solid holdup could theoretically have affected the tracer concentration measurements, they had a negligible effect.

Experimental Results and Discussion

Size and shape of the biobone particles

The size of the particles was characterized with Martin's diameter, which is the average of the four "diameters" taken at angles of 0, 45, 90 and 135° (a "diameter" goes from edge

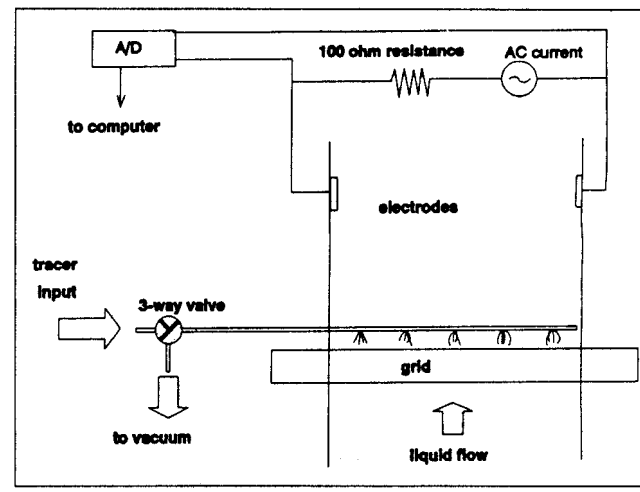

Figure 3. Tracer injection system for residence time distribution studies.

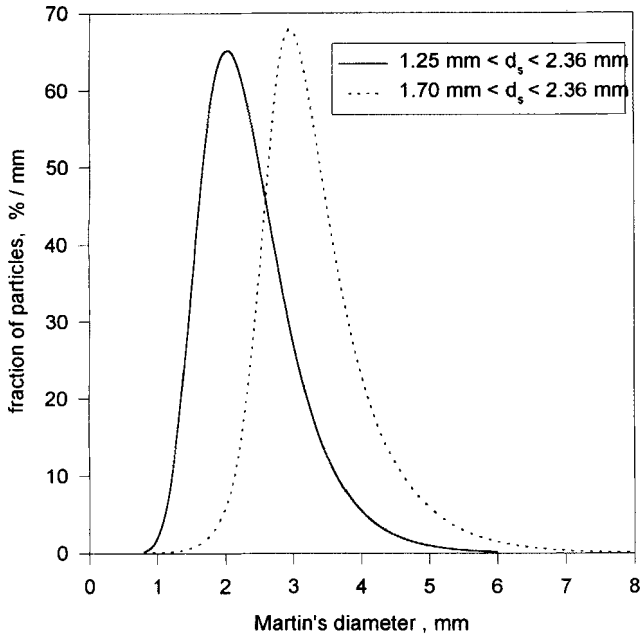

Figure 4. Differential number distributions of Martin's diameter for two Biobone screened fractions for fluidization experiments.

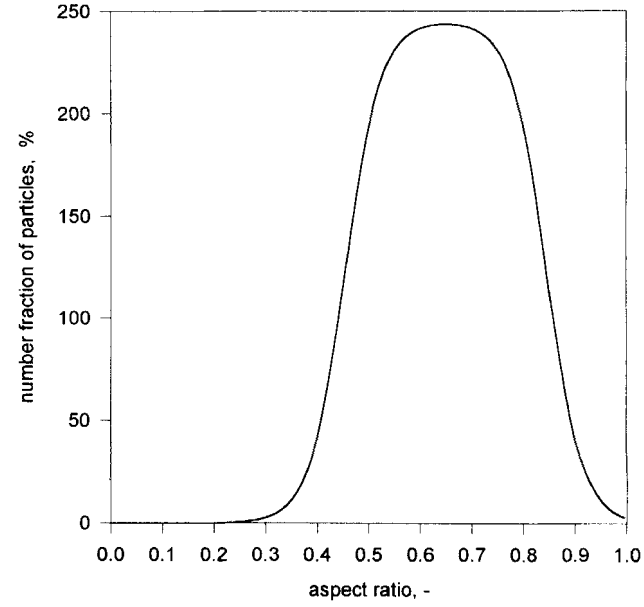

Figure 5. Differential number distribution of the aspect ratio of Biobone particles (1.25 mm $< d_s <$ 2.36 mm).

to edge, through the center of gravity of the particle). This diameter was directly provided by the Brinkman particle-size analyzer. Figure 4 shows that the distribution was wide for both size cuts, namely 1.25 mm $< d_s <$ 2.36 mm and 1.70 mm $< d_s <$ 2.36 mm. Although there was a negligible fraction of particles with a Martin's diameter smaller than the lower screen size, d_s, used during sieving, at least 50% of the particles had a Martin's diameter larger than the top screen size. This confirms that the particles were elongated splinters as shown in the photograph (Figure 1).

The shape of a particle was characterized with its aspect ratio, which is defined as the ratio of its smallest "diameter" to its largest "diameter." For example, a sphere would have an aspect ratio of 1.0. Figure 5 shows that the biobone particles have an aspect ratio ranging from 0.3 to 1.0, with an average of about 0.65, which further confirms their needle-like shape.

Terminal free-falling velocity of biobone particles

The correlations proposed by Ganser (1993) and Haider and Levenspiel (1989) for the terminal velocity of nonspherical particles did not provide reliable predictions of the biobone data. This probably resulted from the highly irregular shape of the biobone particles.

Although the biobone particles had a complex shape, a very good correlation was obtained between their terminal free-falling velocity and their Martin's diameter. Figure 6 displays a linear correlation between Martin's diameter d_M and the velocity-equivalent diameter d_{eq}, defined as the diameter of a sphere of the same density as the particle that has the same terminal velocity as the particle. The correlation is shown by Eq. 1, where d_{eq} and d_M are expressed in m:

$$d_{eq} = 0.4374\ d_M + 5.48 \times 10^{-5} \quad (\text{for } d_M > 0.001 \text{ m}). \quad (1)$$

This means that the terminal velocity of a Biobone particle can be estimated from the results of automatic shape analysis, as performed, in this study, with the Brinkman Particle Size Analyzer, model PSA 2010.

Angle of internal friction of biobone particles

The angle of internal friction was about 80° for both dry and wet biobone. This contrasts with noncohesive glass beads,

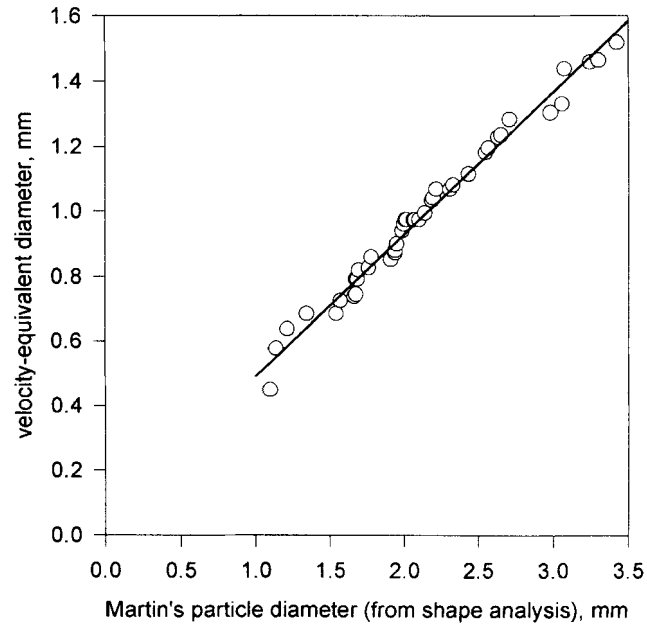

Figure 6. Diameter of the sphere with the same terminal free-falling velocity as a Biobone particle vs. Martin's diameter of the Biobone particle.

which have an angle of internal friction of only 50 to 60°. Screening the biobone did not greatly affect its angle of internal friction, since the raw biobone and the two screened size fractions used for the fluidization experiments gave similar results. The flaky, needlelike biobone particles snag at each other and form a very cohesive structure that is indicated by their high angle of internal friction. Although no information is available on the relationship between liquid fluidization behavior and the angle of internal friction, gas fluidization of powders with an angle of internal friction larger than 80° is characterized by poor gas–solid contact since most of the gas flows through channels and bypasses the solids. The large angle of internal friction obtained with biobone particles suggested that channeling may occur in liquid fluidization of biobone particles.

Attrition of the biobone particles

Preliminary experiments indicated that while biobone particles were much less prone to attrition than traditional immobilization supports, appreciable attrition occurred at high liquid velocities. Uninterrupted fluidization for nine days at a superficial liquid velocity of 7.7 cm/s caused appreciable attrition. The mean Martin's diameter of the bed particles was reduced by about 30% from 3.1 to 2.2 mm. The coefficient of variation of their size distribution went from 20 to 30%. The shape of the particles, however, was not affected by attrition. The prime attrition mechanism was therefore breakage and not erosion, which would have made the particles rounder.

A surprising consequence of attrition was to increase the minimum liquid velocity required to achieve complete fluidization. Attrition, by making the size distribution wider, increased the tendency of the particles to segregate by size in the fluidized bed. A larger liquid velocity was thus required to induce enough agitation and prevent segregation and defluidization of the larger particles.

Entrainment of biobone particles from the fluidized bed

Figure 7 shows that, as expected, the average diameter of the particles entrained in the freeboard, at a height of about 2.5 times the fluidized-bed height, increased with the superficial liquid velocity. Figure 7 also shows that the size distribution of the bed particles had surprisingly little effect on the size of the entrained particles. In all cases, no entrained particles had a terminal free-falling velocity larger than the superficial liquid velocity; this indicates that any irregularity in the radial liquid velocity profile inside the bed had been smoothed out by the time the liquid reached a height of 2.5 times the bed height. In all cases, the aspect ratio distribution of the entrained particles was essentially the same as that of the bed particles; there was no preferential entrainment of particles of a certain shape and entrainment should not affect the shape of the remaining bed particles.

Figure 8 shows that the flux of entrained particles increased exponentially with the superficial liquid velocity. Surprisingly, the size distribution of the bed particles did not significantly affect the entrained particles flux. This means that the fraction of entrainable particles in the bed, that is, the fraction of particles with a terminal free-falling velocity smaller than the superficial liquid velocity, did not affect the

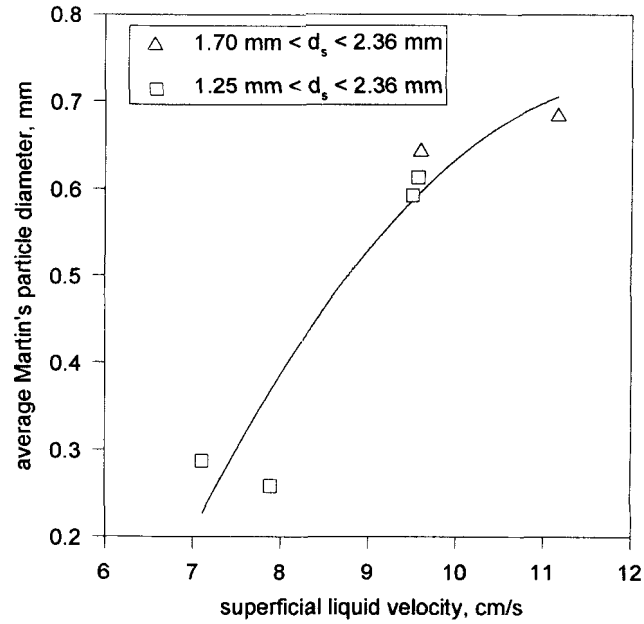

Figure 7. Arithmetic number-average of Martin's diameter of entrained Biobone particles as a function of the superficial liquid velocity.

entrained flux. For example, at a liquid superficial velocity of 9.6 cm/s, the entrained flux was about the same for both sets of bed particle-size distribution, although the fraction of entrainable particles went from 1.2% for the bed of coarser particles to 32% for the bed that contained both fine and coarse particles.

Since the shape, size, and flux of entrained particles are not affected by the removal from the bed of particles with screen sizes ranging from 1.25 to 1.70 mm, they should not be removed. While removing the particles smaller than 1.25 mm

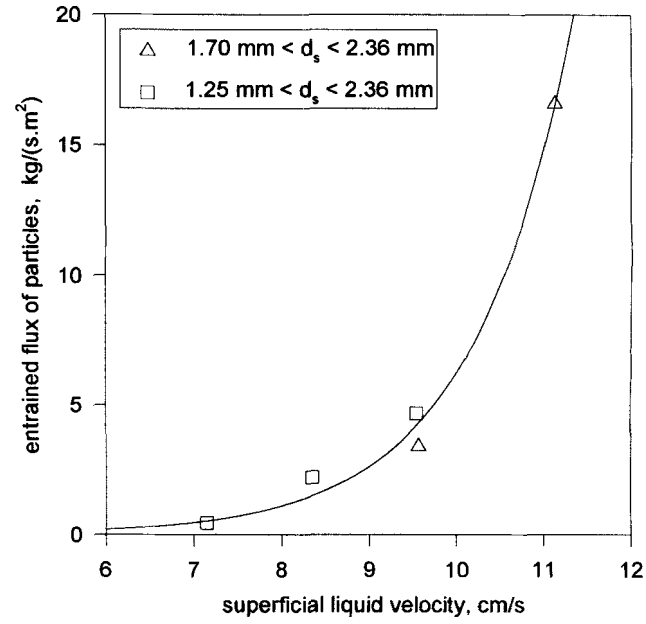

Figure 8. Effect of the superficial liquid velocity on the flux of entrained particles.

and larger than 2.36 mm was necessary to achieve fluidization at a reasonable velocity, further removal of particles between 1.25 mm and 1.70 mm increased the minimum velocity required to fluidize the bed. Since entrainment losses increase exponentially with the liquid velocity, the bed composition should be such that the bed is fluidized at a low velocity. A detailed study of the bed fluidization characteristics was thus performed to identify the lowest liquid velocity that achieves smooth fluidization.

Visual observations of the fluidization of biobone particles

Extensive video recordings of the fluidized bed were analyzed and established that raw, unscreened biobone was unsuitable for fluidization. Particle segregation by size was such that too large a liquid velocity was required to achieve complete fluidization. At such a large velocity, entrainment and attrition rates would be too large for sustained continuous operation.

The screened biobone fractions (1.25 mm $< d_s <$ 2.36 mm and 1.70 mm $< d_s <$ 2.36 mm) were much more appropriate for fluidization. In both cases, the bed was observed to go through the following five stages as the liquid velocity was increased:

1. At low liquid velocities, the bed particles were completely fixed.
2. As the liquid velocity was increased past the minimum fluidization velocity, most of the bed became fluidized, although a significant fraction remained defluidized. Increasing the liquid velocity did not eliminate the defluidized zones as the extra liquid flow rate went to form channels through which the liquid flowed at high velocity, bypassing most of the solid particles. Channeling should be avoided since it impairs the particle–liquid contact that is required for a satisfactory operation of the bioreactors that use immobilization technology.
3. Further increases in the liquid velocity led to a bed with few channels and no defluidized zones. This attractive behavior could only be maintained over a narrow range of liquid velocities.
4. Increasing the liquid velocity, while maintaining complete fluidization, led to the reappearance of numerous channels through which most of the liquid flowed. Although some solids were present in the channels, they represented a small fraction of the bed solids that were thus bypassed by most of the liquid flow. Moreover, the solids present in the channel probably underwent significant and undesirable attrition.
5. Finally, a very high velocities of nearly 10 cm/s, complete fluidization was achieved with few channels. Continuous operation at such velocities would be impractical since it would result in large entrainment and attrition losses.

Minimum fluidization conditions

Figure 9 shows how the vertical pressure gradient in the bed varied with the superficial liquid velocity. Three different measurement procedures were used. With the first procedure, the liquid velocity was steadily increased. The significant peak in pressure gradient obtained with this procedure between 4 and 6 cm/s liquid superficial velocity results from the mechanical interlocking of the needlelike biobone particles that had to be overcome by a drag force larger than the

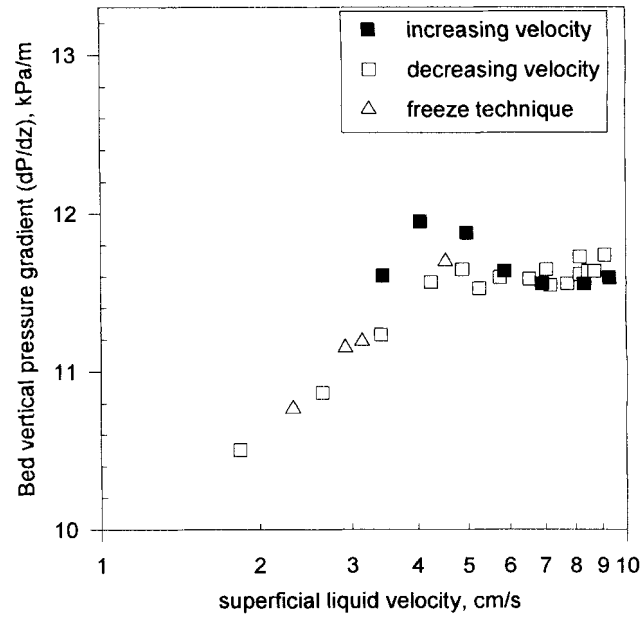

Figure 9. Effect of the superficial liquid velocity on the vertical pressure gradient in the bed of Biobone particles (1.25 mm $< d_s <$ 2.36 mm).

net weight of the particles to achieve fluidization. With the second procedure, the liquid velocity was steadily decreased from an initial velocity of nearly 10 cm/s. Since the transition between fluidized and fixed states was approached from the fluidized side, mechanical interlocking was not a problem and there was no peak in pressure gradient. The third "freeze" procedure was used to limit eventual particle segregation as the bed went from fluidized to fixed state. The bed was fluidized at 10 cm/s and the liquid flow was suddenly switched off. The liquid velocity was then increased to the desired value. Figure 9 shows that similar results were obtained with the second and third procedures.

Figure 9 did not display a clear, sharp transition between the fixed and fluidized states, a different plot was used. A parameter α, which is defined by Eq. 2, is used:

$$\alpha = -dP/(\rho_L g dz) - \epsilon_s(\rho_s/\rho_L), \tag{2}$$

where the solid holdup ϵ_s was obtained from the total mass of solids and the bed height, as determined from the pressure profile and confirmed by visual observations.

In the fluidized state, α is equal to the liquid holdup. Figure 9 shows that the increasing velocity data cannot be used to obtain the minimum fluidization velocity. Using data obtained with the decreasing velocity and "freeze" procedures, the minimum fluidization velocity was found to be 4.65 cm/s, as shown in Figure 10. For the bed containing solids with screen sizes between 1.25 and 2.36 mm, the minimum fluidization velocity was 4.10 cm/s.

As shown in Figure 11, the bed voidage at minimum fluidization was obtained by plotting, in log-log coordinates, $\alpha^2/(1-\alpha)$ against the ratio of the superficial velocity to the minimum fluidization velocity. The solid voidage at minimum fluidization conditions was 0.80 for the solids with screen sizes between 1.25 and 2.36 mm, and 0.78 for the solids with screen

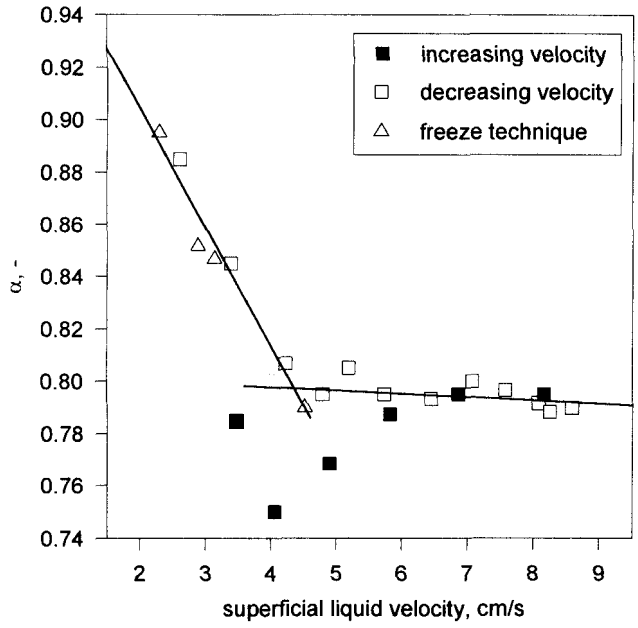

Figure 10. Determination of the minimum fluidization velocity for Biobone particles (1.70 mm $< d_s <$ 2.36 mm).

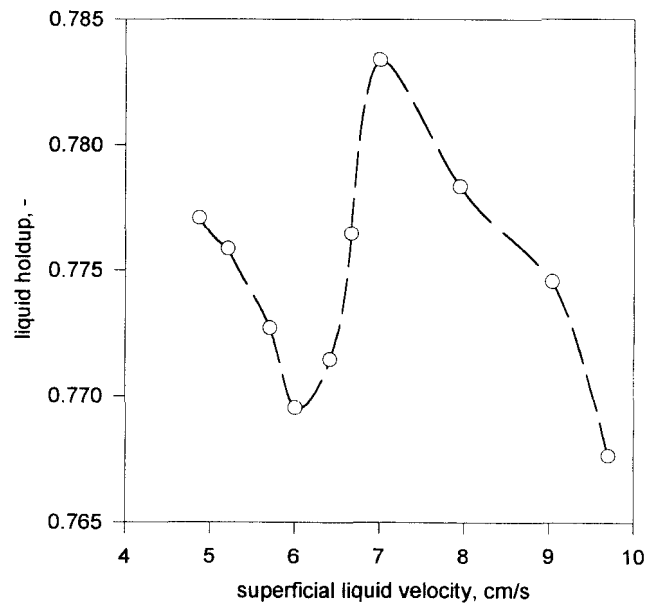

Figure 12. Effect of the superficial liquid velocity on the liquid holdup in the fluidized bed of Biobone particles (1.70 mm $< d_s <$ 2.36 mm).

sizes between 1.70 and 2.36 mm. These values are much larger than the typical value of about 0.4 for a minimally fluidized bed of spherical particles. The cohesive forces between biobone particles strengthen the open structure of their beds.

Bed expansion and liquid holdup

Figure 12 shows how the liquid holdup in the fluidized bed varied with the liquid superficial velocity. With spherical particles, as the superficial velocity is increased, the fluidized bed steadily expands and the liquid holdup increases to keep the drag force of the liquid on a bed particle equal to the net weight of this particle, where the net weight is defined as the difference between the weight and the buoyancy force. The drag force acting on a sphere in a fluidized bed may be approximately assumed proportional to $C_D T U_L/\epsilon_L$, where C_D is the drag coefficient, U_L the superficial velocity, T the tortuosity, and ϵ_L the liquid holdup. With spherical particles, the liquid holdup increases by about 25% as the liquid velocity is doubled.

With biobone, however, the situation was completely different. Although the scale of Figure 12 amplifies the nonmonotonic variations of the holdup, the liquid holdup varied by less than 2% as the superficial velocity was doubled. Two effects combined to minimize variations in liquid holdup. First, the liquid holdup ϵ_L did not have to increase to keep the drag force of the liquid on a bed particle equal to the net weight of this particle. Instead, the flaky biobone particles realigned themselves so as to be parallel to the liquid flow, thus reducing the drag coefficient C_D. Second, as the superficial velocity was increased, a large fraction of the liquid bypassed the particles and flowed at high speed through channels that did not contribute much to the bed expansion.

Attempts to fit to the biobone data a model developed for the particulate fluidization of irregularly shaped particles by Molerus and Schweinzer (1989) were unsuccessful. The Biobone fluidized beds were therefore not in the particulate fluidization regime, which confirms the importance of channeling in the fluidized beds of biobone particles.

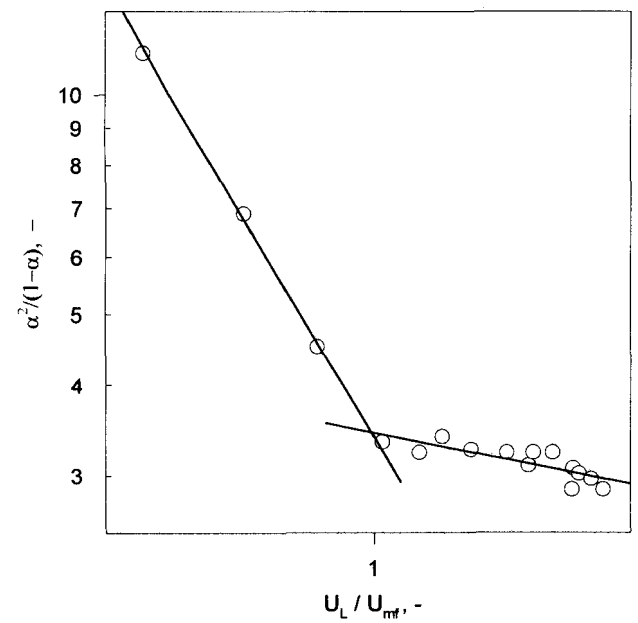

Figure 11. Determination of the bed voidage at minimum fluidization of Biobone particles (1.70 mm $< d_s <$ 2.36 mm).

Development of a new channeling index

A new channeling index was developed to quantify the extent of channeling from tracer residence time distribution

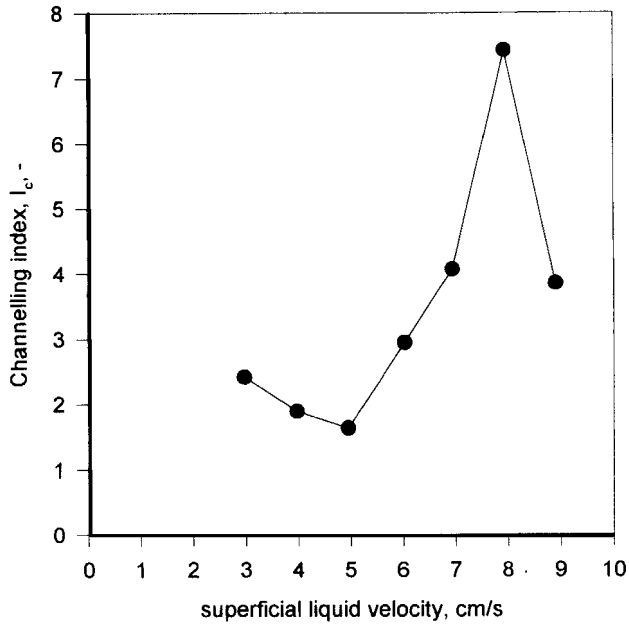

Figure 13. Effect of the superficial liquid velocity on channeling in the fluidized bed of Biobone particles (1.70 mm $< d_s <$ 2.36 mm).

measurements in the biobone fluidized-bed bioreactor. It was defined as:

$$I_c = -1 + \frac{1}{\tau_{ADM}} \int_0^\infty f(t)t\,dt, \tag{3}$$

where

$f(t)$ = tracer response of the system to a perfect impulse of tracer
τ_{ADM} = average time of the tracer response if the system could be represented with the axially dispersed plug-flow model

This average time is only equal to the mean residence time when the system boundaries are closed, which is not the case here. It was obtained by fitting the axial dispersion model equations to the measured tracer response data.

The axially dispersed plug-flow model is the most popular model for the liquid residence time distribution in fixed and fluidized beds (Kikuchi et al., 1984). In the absence of channeling, this model should apply to the tracer response of the biobone bed and the following should be verified:

$$\tau_{ADM} = \int_0^\infty f(t)t\,dt \qquad \text{(no channeling)}, \tag{4}$$

which would give a channeling index of zero.

In the presence of channeling, the liquid that moves quickly through the channels does not remain long in the detector field. Its contribution to the tracer response is thus underestimated and the measured tracer response is skewed toward the longer times [Levenspiel and Turner (1970) and Briens et al. (1994) review the general problems associated with tracer measurements]. Consequently,

$$\int_0^\infty f(t)t\,dt > \tau_{ADM} \tag{5}$$

and the channeling index is no longer zero. The larger the channeling index, I_c, the more severe the channeling.

With downstep experiments, the tracer response function is no longer $f(t)$ but $y(t)$, and the channeling index can be expressed by Eq. 6:

$$I_c = -1 + \frac{1}{\tau_{ADM}} \int_0^\infty y(t)\,dt. \tag{6}$$

Figure 13 shows the variation of the channeling index with the superficial liquid velocity. In the fixed bed, channeling was moderate and was reduced as the velocity was increased and larger pressure gradients led to a more uniform distribution of liquid through the bed. In the fluidized bed, however, channeling sharply increased with the liquid velocity, reaching a maximum for a liquid velocity of about 8 cm/s and decreasing as the liquid velocity was further increased. Since large liquid velocities cause large entrainment and attrition losses, the only practical way to reduce channeling is to operate at a liquid velocity just above the minimum fluidization velocity.

Conclusions

Irregularly shaped biobone particles used in this study had a size range 1.25 mm to 2.36 mm and an average aspect ratio of 0.65, compared to spherical particles, which have an aspect ratio of 1.0. They were fluidized with water in a bioreactor column. The needlelike shape of the biobone particles resulted in fluidization behavior that was found to be much different from that observed and reported in the literature for spherical particles. An empirical linear correlation was developed, for the biobone particles, between the Martin's diameter and the velocity-equivalent particle diameter based on terminal velocity measurements. It was found that the flux of entrained biobone particles increased exponentially with the superficial liquid velocity, and the size distribution of the particles in the bed did not significantly affect the entrained particles flux. A new parameter, α, was developed to distinguish the transition between fixed and fluidized states of the biobone particles in the column. In the fluidized state, α is equal to the liquid holdup. Residence time distribution measurements were made and a new channelling index, I_c, was developed to quantify channeling in the column when the Biobone particles were in fixed- or fluidized-bed state. Biobone is an excellent new matrix of commercial importance for the immobilization of a large number of biocatalysts used in fluidized bioreactor systems. More work is needed to fully characterize the fluidization behavior of Biobone particles including work in three-phase systems, solid–water–air, which will open up more commercial applications of Biobone to aerobic biological systems, such as wastewater treatment.

Acknowledgments

Argyrios Margaritis, Cedric Briens, and Maurice Bergougnou wish to acknowledge the support through their individual research grants awarded by the Natural Sciences and Engineering Research Council (NSERC) of Canada.

Notation

g = gravity acceleration, m/s^2
P = pressure, Pa
t = time, s
z = height above the grid, m
ρ_L = liquid density, kg/m^3
ρ_s = solid particle density, kg/m^3

Literature Cited

Briens, C. L., A. Margaritis, and G. Wild, "A New Stochastic Model and Measurement Errors in Residence Time Distributions of Multiphase Reactors," *Chem. Eng. Sci.*, **50**, 279 (1995).

Del Pozo, M., C. L. Briens, and G. Wild, "Effect of Liquid Coalescing Properties on Mass Transfer, Heat Transfer and Hydrodynamics in a Three-Phase Fluidized Bed," *Chem. Eng. J.*, **55**, 1 (1994).

Del Pozo, M., C. L. Briens, and G. Wild, "Effect of Column Inclination on the Performance of Three-Phase Fluidized Beds," *AIChE J.*, **38**, 1206 (1992).

Ellis, N., "Liquid Fluidization Characteristics of Biobone Particles," M.E.Sc. thesis, Dept. of Chemical and Biochemical Engineering, University of Western Ontario, London, Ontario, Canada, N6A 5B9 (1993).

Fan, L. S., *Gas-Liquid-Solid Fluidization Engineering*, Butterworths, Boston (1989).

Findlay, C. J., K. L. Parkin, and R. Y. Yada, "Bone as a Solid Support for the Immobilization of Enzymes," *Biotech. Lett.*, **8**(9), 649 (1986).

Ganser, G. H., "A Rational Approach to Drag Prediction of Spherical and Nonspherical Particles," *Powder Technol.*, **77**, 143 (1993).

Galy-Jammou, P., C. Briens, M. Bergougnou, and J. F. Large, "Local Particle Heat Transfer and Hydrodynamics in Three-Phase Fluidized Beds with Light Particles," Int. Conf. on Gas-Liquid-Solid Reactor Eng., Cambridge, UK (Mar., 1995).

Gee, D. A., and W. R. Ramirez, "A Flavour Model for Beer Fermentation," *J. Inst. Brew.*, 321 (Sept.–Oct., 1994).

Haider, A., and O. Levenspiel, "Drag Coefficient and Terminal Velocity of Spherical and Nonspherical Particles," *Powder Technol.*, **58**, 63 (1989).

Kikuchi, K., H. Konno, S. Kakutani, T. Sugawara, and H. Ohashi, "Axial Dispersion of Liquid in Liquid Fluidized Beds in the Low Reynolds Number Region," *J. Chem. Eng. Japan*, **17**, 362 (1984).

Levenspiel, O., and J. C. R. Turner, "The Interpretation of Residence-Time Experiments," *Chem. Eng. Sci.*, **25**, 1605 (1970).

Manji, B., R. Y. Yada, D. J. Findlay, and K. L. Parkin, "Optimization for the Immobilization of Milk-Clotting Proteases to Granular Bone," *Food Biotechnol*, **2**(1), 43 (1988).

Margaritis, A., and F. Merchant, "Advances in Ethanol Production Using Immobilized Cell Systems," *CRC Crit. Rev. Biotechnol.*, **1**(4), 339 (1984).

Margaritis, A., and J. B. Wallace, "Novel Bioreactor Systems and their Applications," *Bio/Technology*, **2**, 447 (1984).

Margaritis, A., D. teBokkel, and M. El-Kashab, "Repeated Batch Fermentation of Ethanol Using Immobilized Cells of *Saccharomyces cerevisiae* in a Fluidized Bioreactor System," *Biological Research on Industrial Yeasts*, G. G. Stewart, I. Russell, R. D. Klein, and R. R. Hiebsch, eds., CRC Press, Boca Raton, FL, p. 121 (1987).

Merchant, F. J. A., A. Margaritis, J. B. Wallace, and A. Vardanis, "A Novel Technique for Measuring Solute Diffusivities in Entrapment Matrices used in Immobilization," *Biotechnol. Bioeng.*, **30**, 936 (1987).

Molerus, O., and J. Schweinzer, "Resistance of Particle Beds at Reynolds Numbers up to $Re \approx 10^4$," *Chem. Eng. Sci.*, **44**, 1071 (1989).

Negishi, S., S. Sato, S. Mukataka, and J. Takahashi, "Utilization of Powdered Pig Bone as a Support for Immobilization of Lipase," *J. Ferment. Bioeng.*, **67**(5), 350 (1989).

Schafhauser, D. Y., and K. B. Storey, "Fructose Production, Co-Immobilized Amyloglucosidase, Pullulanase, and Glucose Isomerase on Biobone," *Appl. Biochem. Biotechnol.*, **36**, 63 (1992).

Weuster-Botz, D., "Continuous Ethanol Production by Zymomonas mobilis in a Fluidized Bed Reactor: I. Kinetic Studies of Immobilization in Macroporous Glass Beads," *Appl. Microbiol. Biotechnol.*, **39**, 679 (1993).

Manuscript received Dec. 5, 1994, and revision received Feb. 17, 1995.